Aeromechanical Stability Analysis of a Hybrid Heavy Lift Multirotor Vehicle in Hover

C. Venkatesan* and P. P. Friedmann†
University of California, Los Angeles, California

Hybrid heavy lift airship (HHLA) is a proposed candidate vehicle aimed at providing heavy lift capability at low cost. This vehicle consists of a buoyant envelope attached to a supporting structure to which four rotor systems are attached. Nonlinear equations of motion capable of modeling the dynamics of this coupled multirotor/support-frame vehicle system have been developed. Using these equations, an aeromechanical stability analysis was performed in order to identify potential instabilities for this type of vehicle. The coupling between various blade, supporting structure, and rigid body modes is identified. Furthermore, the effects of changes in buoyancy ratio (buoyant lift/total weight) on the dynamic characteristics of the vehicle were studied.

Nomenclature

BR = buoyancy ratio (buoyant lift/total weight of the vehicle)
$[C]$ = damping matrix
C_T = thrust coefficient of the rotor
f = rotating natural frequency
F_x, F_y, F_z = forces along x,y,z directions of the body axes
I_{xx}, I_{yy} = rotary inertia of the vehicle in roll and pitch, respectively
$[K]$ = stiffness matrix
K_{SBXY}, K_{SBXZ} = supporting structure bending stiffness in x-y (horizontal) plane and in x-z (vertical) plane, respectively, (in fundamental mode)
K_{ST} = supporting structure torsional stiffness (in fundamental mode)
$K_\beta, K_\zeta, K_{\phi B}$ = root spring constant of the blade in flap, lag, and torsion, respectively
$K_{\phi C}$ = control system stiffness
K_ϕ = equivalent spring stiffness in torsion of the blade
$[M]$ = mass matrix
M_x, M_y, M_z = moments about x,y,z axes acting on the vehicle
M_β, M_ζ, M_ϕ = blade root moments in flap, lag, and torsion, respectively
N = number of blades in a rotor ($N>2$)
P_z^s = static buoyancy on the envelope
$\{q\}$ = generalized coordinate vector
R_x, R_y, R_z = rigid body perturbational motion in x,y,z directions, respectively
s_k = kth eigenvalue ($\sigma_k \pm j\omega_k$)
T_1, T_2 = thrust developed by rotor systems R_1 and R_2, respectively
W = total weight of the vehicle
β_k, ζ_k, ϕ_k = flap, lead-lag, and torsion angles of the kth blade
$\beta_{k0}^i, \zeta_{k0}^i, \phi_{k0}^i$ = equilibrium angles in flap, lag, and torsion of the kth blade in the ith rotor system $i=1,2$
β_0, ζ_0, ϕ_0 = equilibrium angles in flap, lag, and torsion, respectively
$\Delta\beta_k, \Delta\zeta_k, \Delta\phi_k$ = perturbational quantities in flap, lag, and torsion, respectively
β_M, ζ_M, ϕ_M = generalized coordinates for collective flap, lag, and torsion modes, respectively
$\beta_{-M}, \zeta_{-M}, \phi_{-M}$ = generalized coordinates for alternating flap, lag, and torsion modes, respectively
$\beta_{1c}, \zeta_{1c}, \phi_{1c}$ = generalized coordinates for 1-cosine flap, lag, and torsion modes
$\beta_{1s}, \zeta_{1s}, \phi_{1s}$ = generalized coordinates for 1-sine flap, lag, and torsion modes
ϵ = basic order of magnitude for blade slopes employed in ordering scheme
λ = inflow ratio
ω_k = modal frequency in kth mode (imaginary part of s_k)
$\bar{\omega}_{SBXY}$ = nondimensional uncoupled fundamental bending frequency of the supporting structure in x-y plane
$\bar{\omega}_{SBXZ}$ = nondimensional uncoupled fundamental bending frequency of the supporting structure in x-z plane
$\bar{\omega}_{ST}$ = nondimensional uncoupled fundamental torsion frequency of the supporting structure
Ω = rotor rpm
σ_k = kth modal damping (real part of s_k)
σ = solidity ratio
θ_0, θ = collective pitch of the blade
θ_0^i = collective pitch setting for the ith rotor
$\theta_x, \theta_y, \theta_z$ = perturbational rotation in roll, pitch, and yaw, respectively
ξ_1, ξ_2 = generalized coordinate for the fundamental mode bending of the supporting structure in x-y plane and x-z plane, respectively
ξ_3 = generalized coordinate for the fundamental torsion mode of the supporting structure
$\bar{(\ )}$ = nondimensional quantity

Presented as Paper 84-0987 at the AIAA/ASME/ASCE/AHS 25th Structures, Structural Dynamics and Materials Conference, Palm Springs, CA, May 14-16, 1984; received July 8, 1984; revision received April 12, 1985.

*Assistant Research Engineer, Mechanical, Aerospace and Nuclear Engineering Department.
†Professor of Engineering and Applied Science, Mechanical, Aerospace and Nuclear Engineering Department.

I. Introduction

HYBRID heavy lift airship (HHLA) or hybrid heavy lift helicopter is a proposed candidate vehicle for providing heavy lift capability. Potential applications of this vehicle are for logging, construction, and military heavy lift. These vehicles combine buoyant envelope lift with lift and control forces generated by a multirotor system. A rough sketch of a typical HHLA vehicle is shown in Fig. 1. A full-scale test vehicle is currently under construction and testing by Piasecki Aircraft Co.[12] Recent studies on HHLA-type vehicles dealt with the overall dynamic stability and control of the vehicle under the assumption that it behaves like a rigid body having six degrees of freedom.[1,2] However, the aeroelastic stability of the rotor and the aeromechanical stability of the coupled rotor/support system, as well as the interaction of the buoyant lift with these vehicle dynamic characteristics, have not been considered in the literature before. Therefore it is reasonable to consider these topics so that potential aeroelastic instability modes and structural dynamic aspects of such vehicles can be simulated and identified in the design process.

The main objectives of this paper are to develop a fundamental understanding of the aeroelastic and aeromechanical problems that can be encountered in a HHLA-type vehicle due to such unique features as buoyancy, multiple rotor systems, flexible supporting structure, and underslung load.

The study is based on a *simplified model* of a HHLA-type vehicle, in which the salient feature are still retained. These simplifying assumptions consists of using *two rotor systems instead of four* and a beam-type structure representing the flexible supporting structure (Fig. 1), which in reality consists of a three-dimensional frame (or truss). The essential features of this configuration, illustrated in Fig. 2, are described below:

1) Two rotor systems, providing lift, each having arbitrary number of blades $N(N>2)$, are attached rigidly to the two ends of a flexible supporting structure.

2) The flexible supporting structure is capable of bending in two orthogonal planes (horizontal and vertical), and it can also twist about its longitudinal axis.

3) An envelope providing buoyant lift, acting at its center of buoyancy, is attached at the center of the supporting structure.

4) Two masses which represent helicopter fuselages, are attached at the two ends of the flexible structure.

5) A weight W_{UN} simulating an underslung load is attached to the structure.

The dynamic equations of motion for this model were derived in Ref. 3.

This paper deals primarily with the aeroelastic and aeromechanical stability analysis of an HHLA type of vehicle, shown in Fig. 2. Based on a careful parametric study, the various blade and vehicle modes have been identified. The physical interpretation of the various eigenvalues is determined from a systematic study of the eigenvalue changes caused by variations of the vehicle modes is identified. Finally, vehicle stability is analyzed at different buoyancy ratios (BR = buoyancy of the envelope/total weight of the vehicle) to determine the influence of buoyancy on the aeromechanical stability of the vehicle.

II. Formulation of Equations of Motion

Recent research on rotary-wing aeroelasticity[4] has indicated that geometrically nonlinear effects due to moderate blade deflections are important for this class of problems. Thus a proper treatment of rotary-wing aeroelastic problems requires the development of a consistent mathematical model, which includes the geometrically nonlinear effects associated with finite blade slopes in the aerodynamic, inertial, and structural operators. Retention of the nonlinear terms is based on an ordering scheme.[3,4] All the important parameters of the problem are assigned orders of magnitude in terms of a nondimensional quantity ϵ, which represents the typical blade slope ($0.1<\epsilon<0.15$). The ordering scheme consists of neglecting terms of the order $0(\epsilon^2)$ when compared to unity, i.e., $1+\epsilon^2 \simeq 1$.

The most important assumptions used in formulating the equations of motion are: 1) each rotor consists of three blades or more; 2) the rotors are lightly loaded; 3) the rotor is in uniform inflow; 4) the rotor blade is modeled as a rigid blade with orthogonal root springs (Fig. 3): this blade model is useful for simulating configurations that are either hingeless or articulated; 5) there is no aerodynamic interference between the rotor and the buoyant envelope; 6) the aerodynamic model used for the rotor is a quasisteady blade element theory based on Greenberg's[5] derivation of unsteady aerodynamic loads on an oscillating airfoil in a pulsating flow; 7) the elastic supporting structure is modeled as a free-free beam for which the bending and torsional structural dynamics are modeled by the corresponding free vibration modes.

The various degrees of freedom considered for the model vehicle are: flap β_k, lead-lag ζ_k, torsion ϕ_k for each blade, rigid body translation R_x,R_y,R_z and rigid body rotation $\theta_x,\theta_y,\theta_z$ of the vehicle as a whole, and the generalized coordinates representing the uncoupled normal modes of vibration of the supporting structure ξ_1,ξ_2,ξ_3. The equation of motion for the blade are obtained by enforcing moment equilibrium, of the various forces on the blade, at the root. The blade equations are written in a hub fixed rotating reference frame, and these equations have periodic coefficients. The rigid body equations of motion are obtained by imposing the force and moment equilibrium of the vehicle. The equations of motion for the elastic modes of the supporting structure are obtained using a normal mode approximation. The complete details and the derivation can be found in Ref. 3.

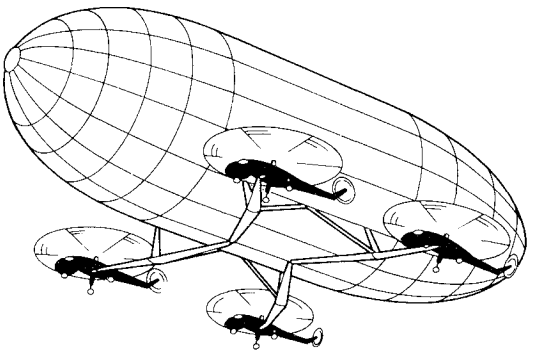

Fig. 1 Hybrid heavy lift airship—approximate configuration.

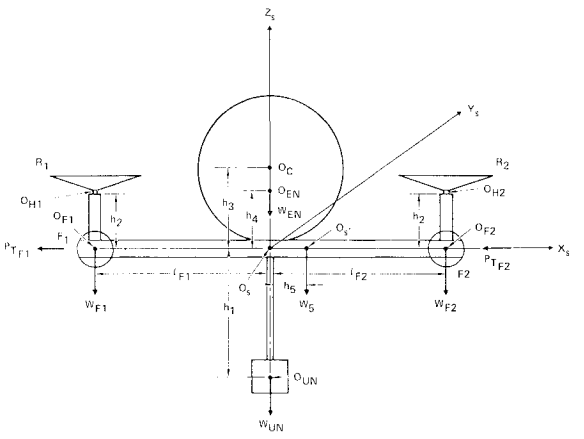

Fig. 2 HHLA model.

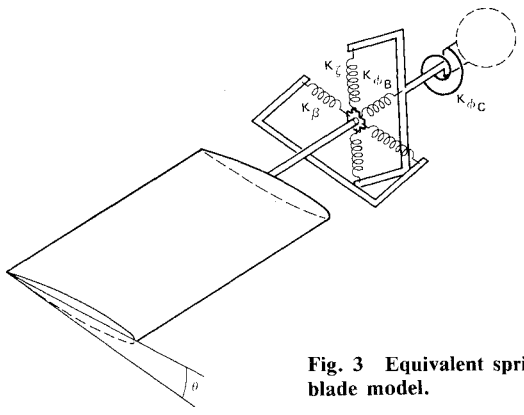

Fig. 3 Equivalent spring restrained blade model.

The final set of equations of motion are nonlinear ordinary differential equations with periodic coefficients. These equations have to be solved so as to determine the aeroelastic and aeromechanical stability characteristics of the vehicle.

III. Method of Solution

The method of solution for the coupled rotors/vehicle problem follows essentially the procedure outlined in Refs. 4 and 6. A brief description of the procedure aimed at determining the aeroelastic and aeromechanical stability characteristics of the vehicle is provided below:

1) Calculation of the equilibrium state of an individual blade and the trim setting of the blade collective pitch angle.

2) Linearization of the nonlinear ordinary differential equations about the equilibrium position (linearized equations will have periodic coefficients).

3) Transformation of the linearized equations with periodic coefficients to linearized equations with constant coefficients, using multiblade coordinate transformation.[7,8]

4) Evaluation of the eigenvalues of the linearized system with constant coefficients to obtain information on the stability of the vehicle.

The four steps described above represent essentially two separate stages of the analysis. The first stage consists of a trim analysis by which the equilibrium position of the blade is determined. Subsequently, in the second stage a stability analysis of the linearized perturbational equation about the equilibrium state is carried out.

Trim or Equilibrium State Solution

In the trim analysis, the force and moment equilibrium of the complete vehicle, together with the moment equilibrium of the individual blade about its root in flap, lead-lag, and torsion, are enforced. It is important to recognize that only the generalized coordinates representing the blade degrees of freedom will have a steady-state value representing the equilibrium position. The generalized coordinates associated with the rigid body motions of the vehicle are essentially perturbational quantities and, hence, their equilibrium or trim values are identically zero. In deriving the equations of motion for the flexible supporting structure, it was assumed that the vibrations of the structure occur about a deflected equilibrium position. The determination of the equilibrium of the supporting structure is unimportant, for the case considered in this study. However, it should be noted that the evaluation of the static equilibrium deflection of the supporting structure could be important in the proper design of the supporting structure.

The kth blade degrees of freedom can be written as

$$\begin{aligned} \beta_k &= \beta_{k0} + \Delta\beta_k(\psi) \quad \text{flap} \\ \zeta_k &= \zeta_{k0} + \Delta\zeta_k(\psi) \quad \text{lead-lag} \\ \phi_k &= \phi_{k0} + \Delta\phi_k(\psi) \quad \text{torsion} \end{aligned} \tag{1}$$

where β_{k0}, ζ_{k0}, ϕ_{k0} are the steady-state values and $\Delta\beta_k$, $\Delta\zeta_k$, $\Delta\phi_k$ are the perturbational quantities.

Linearization of the equations is accomplished by substituting these expressions into the nonlinear coupled differential equations and neglecting terms containing the products or squares of the perturbational quantities. The remaining terms are then separated into two groups: one group of terms contains only the steady-state quantities and constants (i.e., time-independent quantities). These represent the trim or equilibrium equations. For the *case of hover,* these are nonlinear algebraic equations, which represent the force and moment equilibrium equations determining the steady state. The second group contains the time-dependent perturbational quantities and represents the equations of motion about the equilibrium position. These linearized dynamic equations of equilibrium are used for the stability analysis.

The steady-state moment equilibrium equations for the individual blade will have the following symbolic form

$$M_\beta = f_1^i(\beta_{k0}^i, \zeta_{k0}^i, \phi_{k0}^i, \theta_0^i) = 0 \tag{2}$$

$$M_\zeta = f_2^i(\beta_{k0}^i, \zeta_{k0}^i, \phi_{k0}^i, \theta_0^i) = 0 \tag{3}$$

$$M_\phi = f_3^i(\beta_{k0}^i, \zeta_{k0}^i, \phi_{k0}^i, \theta_0^i) = 0 \tag{4}$$

where $i = 1,2$ refer to the two rotor systems R_1 and R_2, respectively, and k refers to the kth blade in the ith rotor system. For the case of hover all the blades in one particular rotor system will have the same steady-state values (i.e., equilibrium quantities). Thus the subscript k can be deleted.

The equations of steady-state equilibrium for the complete vehicle can be written as

$$F_z = T_1 + T_2 + P_z^s - W = 0 \tag{5}$$

$$M_y = 0 \tag{6}$$

where T_1 and T_2 are the thrust developed by the two rotor systems R_1 and R_2, respectively, P_z^s is the static buoyancy due to the envelope, and W is the weight of the complete vehicle. The quantities T_1 and T_2 are functions of the steady-state flap, lead-lag and torsion angles, collective pitch angles, and the operating conditions of the rotor. Equation (6) for M_y consists of the pitching moments developed by the thrust due to the rotors and the gravity loads acting on the various components.

Equations (2-4), and (5), and (6) are nonlinear algebraic equations. There are a total of eight equations and eight variables (β_0^i, ζ_0^i, ϕ_0^i, θ_0^i; $1 = 1,2$). These eight equations are solved iteratively, using the Newton-Raphson method, to obtain the steady-state values. Failure to converge during iteration is attributed to divergence or static instability of the blade.

In deriving the equations of motion, the inflow ratio λ is assumed to be constant over the rotor disc. The typical value chosen for the inflow ratio is its value at 75% of blade, and is given by[7]

$$\lambda = (\sigma a/16)[-1 + \sqrt{1 + (24\theta_0/\sigma a)}] \tag{7}$$

Description of Stability Analysis

The perturbational equations of motion, linearized about the equilibrium position, can be written in the following form:

$$[M]\{\ddot{q}\} + [c]\{\dot{q}\} + [K]\{q\} = 0 \tag{8}$$

where $\{q\}$ contains all the degrees of freedom representing the blade motion, the rigid body motions of the vehicle, and the flexible modes of the supporting structure.

The matrices $[M]$, $[C]$, and $[K]$ can be identified as representing mass, damping, and stiffness matrices, respectively, and the elements of these matrices are functions of the equilibrium values.

The stability of the vehicle about the trim position is obtained by solving the eigenvalue problem represented by Eq. (8). The eigenvalues of Eq. (8) can be either real or complex conjugate pairs

$$s_k = \sigma_k \pm i\omega_k$$

The complex part of the kth eigenvalues (ω_k) refers to the modal frequency, and the real part (σ_k) refers to the modal damping. The mode is stable when $\sigma_k < 0$, and the stability boundary is represented by $\sigma_k = 0$.

In the present case, the matrices $[M]$, $[C]$, and $[K]$ in the linearized perturbational equations are time-dependent. Hence, the stability analysis can be performed by applying either Floquet theory or by using a multiblade coordinate transformation.[7,8] It is well known that for a coupled rotor/vehicle type of analysis in hover, the multiblade coordinate transformation is successful in eliminating the time-dependent coefficients in the equations of motion. During this transformation the individual blade degrees of freedom will transform into a new set of rotor degrees of freedom. (It is worthwhile mentioning that this transformation is also frequently denoted by the terms Fourier transformation, Coleman transformation and, more recently, rotor plane coordinate transformation.[8]) These rotor degrees of freedom are basically representative of the behavior of the rotor as a whole when viewed from a nonrotating reference frame. The various rotor degrees of freedom are denoted as collective, cyclic and alternating degrees of freedom. For example, in a four-bladed rotor, the flap degree of freedom corresponding to each blade β_k; $k = 1,4$, will transform into collective flap β_M, cyclic flap β_{1c}, β_{1s}, and alternating flap β_{-M} degrees of freedom. Alternating degrees of freedom will appear only when the rotor consists of an even number of blades. In a similar fashion, the lead-lag and torsional degrees of freedom will also transform into corresponding rotor degrees of freedom.

As a result of the application of the multiblade coordinate transformation, the linearized perturbational equations with periodic coefficients will transform into linearized perturbational equations with constant coefficients. Using these equations, with constant coefficients, a stability analysis is performed as described above. The eigenvalues corresponding to the cyclic degrees of freedom of the rotor β_{1c}, β_{1s}, ζ_{1c}, ζ_{1s}, ϕ_{1c}, ϕ_{1s}, are referred in this paper as high-frequency (or progressing) and low-frequency (or progressing or regressing) mode. The designation of high-frequency or low-frequency mode is based on the rotating natural frequency of the mode. Suppose, the rotating natural frequency, say in lead-lag, is f/rev, then the two frequencies corresponding to the cyclic modes ζ_{1c}, ζ_{1s}, will be usually $(f+1)$/rev and $(f-1)$/rev. The mode with the frequency $(f+1)$/rev is called a high-frequency lag mode and the mode corresponding to $(f-1)$/rev is called a low-frequency lag mode. The mode with the frequency f/rev is known as the collective lag mode. Since the HHLA model vehicle (Fig. 2) consists of two rotor systems coupled by a supporting structure, the stability analysis will provide a pair of eigenvalues for each rotor degree of freedom. Hence, for the purpose of identification, in the presentation of the results the rotor modes will be referred to as mode 1 and mode 2, as in collective flap mode 1, collective flap mode 2 and high-frequency flap mode 1 and high-frequency flap mode 2, etc. From a physical point of view, mode 1 represents a situation in which the centers of mass of the two rotors move out of phase, while mode 2 corresponds to in-phase motion of the centers of mass.

IV. Results and Discussion

Validity of the coupled rotor/fuselage model derived in Ref. 3 was confirmed by comparing single-rotor coupled-rotor/fuselage stability results with experimental data.[9] The results indicated that the model is quite accurate.

The stability of the model vehicle, shown in Fig. 2, which represents approximately an HHLA-type vehicle, was analyzed for the case of hover. The various degrees of freedom considered for this problem are flap, lead-lag, torsion (for each blade), rigid body translation R_x, R_y, rigid body rotation θ_x, θ_y, and three normal modes of vibration of the supporting structure. The three normal modes represent the fundamental symmetric bending mode ξ_1 in the horizontal x-y plane, the fundamental symmetric bending mode ξ_2 in the vertical x-z plane, and the fundamental antisymmetric torsion ξ_3 about the longitudinal axis. For a four-bladed rotor there are 31 degrees of freedom in all, namely, 12 rotor degrees of freedom for each rotor, plus 4 rigid degrees of freedom, plus 3 elastic vibration modes of the supporting structure. Hence, a stability analysis for this system will yield

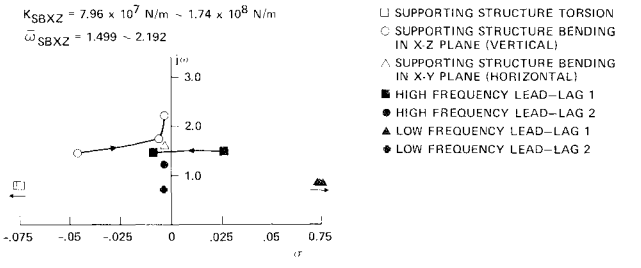

Fig. 5 Variation of nondimensional eigenvalues of blade lead-lag modes and supporting structure bending modes with increase in K_{SBXZ} ($\bar{\omega}_{SBXY} = 1.499$, $\bar{\omega}_{ST} = 1.096$, $I_{xx} = 6.44 \times 10^5$ kg·m^2, $I_{yy} = 2.59 \times 10^6$ kg·m^2, $BR = 0.792$, $C_T = 0.00158$).

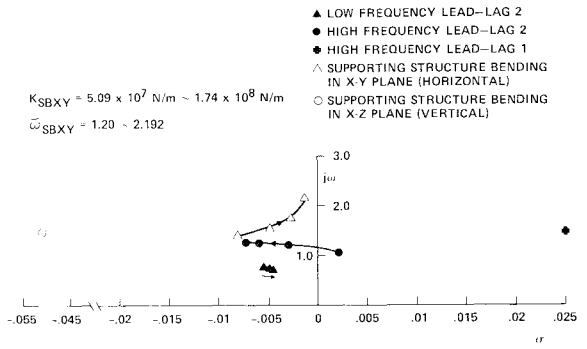

Fig. 4 Variation of nondimensional eigenvalues of blade lead-lag modes and supporting structure bending modes with increase in K_{SBYX} ($\bar{\omega}_{SBXZ} = 1.499$, $\bar{\omega}_{ST} = 1.096$, $I_{xx} = 6.44 \times 10^5$ kg·m^2, 2.59×10^6 kg·m^2, $BR = 0.792$, $C_T = 0.00158$).

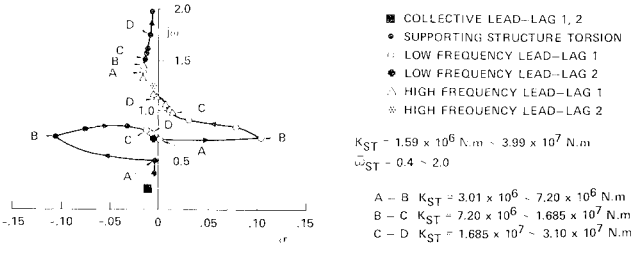

Fig. 6 Variation of nondimensional eigenvalues of blade lead-lag modes and supporting structure torsion mode with increase in K_{ST} ($\bar{\omega}_{SBXY} = \bar{\omega}_{SBXZ} = 2.192$, $I_{xx} = 6.44 \times 10^5$ kg·m^2, $I_{yy} = 2.59 \times 10^6$ kg·m^2, $BR = 0.792$, $C_T = 0.00158$).

62 eigenvalues corresponding to these 31 degrees of freedom. The primary aim is to identify the 62 eigenvalues and relate them to the various modes of the rotor/vehicle assembly. This relatively complicated identification process is based on physical insight gained by performing some preliminary calculations augmented by additional considerations described below:

1) Comparison of the imaginary part of the eigenvalue ω with the uncoupled frequencies of the various modes.

2) Use of an extensive parametric study in which the primary parameters varied are the bending and torsional stiffness of the supporting structure K_{SBXY}, K_{SBXZ}, K_{ST}, combined with the rotary inertia of the vehicle in pitch I_{yy} and roll I_{xx}.

Based on the results obtained in the parametric study, the various eigenvalues and the coupling among different modes are identified. It should be noted that for the case studied, the trim (or equilibrium) quantities are the same because the trim values are independent of the quantities varied in the parametric study. A complete description of this study can be found in Refs. 6 and 10.

For the example problem analyzed, the rotors are articulated and they are identical. In the calculation of the results, it was assumed that the lag damping associated with the lag dampers was equal to zero. Thus, the system is more sensitive than under normal conditions and potential instabilities, which are weak, could be identified. The data used in this study are presented in Appendix A. The results presented below are obtained for the model vehicle without the sling load. Since the two rotors have identical geometric properties and identical operating conditions and, furthermore, the model vehicle possesses a symmetry about y-z plane, the equilibrium angles of the blade are the same for both rotor systems. For the buoyancy ratio of $BR = 0.792$, the thrust coefficient of the rotors is $C_T = 0.00158$. The equilibrium blade angles are: in flap $\beta_0 = 2302$ deg, in lead-lag $\zeta_0 = -3.963$ deg, and in torsion $\phi_0 = -0.115$ deg. The collective pitch angle is $\theta_0 = 4.206$ deg.

The results of the stability analyses are presented in Figs. 4-7. Figure 4 illustrates the variation of the eigenvalues of blade lead-lag modes and the supporting structure bending modes as a result of an increase in the bending stiffness K_{SBXY} of the supporting structure in x-y (horizontal) plane. The bending stiffness K_{SBXY} was increased in increments from 5.09×10^7 N/m to 1.74×10^8 N/m, such that the corresponding uncoupled nondimensional bending frequency in x-y plane ($\bar{\omega}_{SBXY}$) assumed the values $\bar{\omega}_{SBXY} = 1.2$, 1.499, 1.754, 2.192, where the frequencies are nondimensionalized with respect to the rotor speed of rotation Ω, ($\Omega = 217.79$ rpm). The arrows in the figure indicate the direction along which the eigenvalues of the modes change due to an increase in K_{SBXY}. The eigenvalues of the other modes, which are not shown in the figure, remain unaffected by the variation in K_{SBXY}. It can be seen from Fig. 4 that the bending mode, in x-y plane, of the supporting structure is strongly coupled with the high-frequency lag mode 2. The high-frequency lag mode 2, which was initially unstable, becomes more stable as K_{SBXY} is increased. The damping in the bending mode in x-y plane decreases asymptotically with an increase in frequency; furthermore, this mode is always stable. The low-frequency lead-lag mode 2 shows a slight decrease in damping as K_{SBXY} is increased. The eigenvalues corresponding to the bending mode in x-z plane and the high-frequency lag mode 1 are not affected by the changes in K_{SBXY}. However, since these two modes have nearly equal frequencies, it can be seen that the high-frequency lag mode 1 is unstable.

Figure 5 presents the variation of eigenvalues of the blade lead-lag modes and the supporting structure bending modes as a result of an increase in the bending stiffness K_{SBXZ} of the supporting structure in x-z (vertical) plane. The bending stiffness K_{SBXZ} was increased in increments from 7.96×10^6 N/m to 1.74×10^8 N/m and the corresponding nondimensional uncoupled bending frequency in x-z plane ($\bar{\omega}_{SBXZ}$) assumed the values $\bar{\omega}_{SBXZ} = 1.499$, 1.754, 2.192. It can be seen from Fig. 5 that the bending mode in x-z plane is strongly coupled with high-frequency lag mode 1. The high-frequency lag mode 1, which was initially unstable, becomes a stable mode as K_{SBXZ} is increased from 7.96×10^7 N/m ($\bar{\omega}_{SBXZ} = 1.499$) to 1.09×10^8 N/m ($\bar{\omega}_{SBXZ} = 1.754$). But a further increase in K_{SBXZ} to 1.74×10^8 N/m does not affect the eigenvalue corresponding to the high-frequency lag mode 1, indicating that these two modes are decoupled. Damping in the bending mode in x-z plane decreases drastically at the beginning, and once the bending mode and the high-frequency lag mode 1 are decoupled, the decrease in damping of the bending mode in x-z plane is very small. Damping in the torsion mode of the supporting structure and low-frequency lag mode 1 are slightly affected as K_{SBXZ} is increased. Since the torsion mode and the low-frequency lag mode 1 have frequencies close to each other, the figure clearly indicates that the lag mode 1 is unstable. The eigenvalues corresponding to the rest of the modes are unaffected.

Figure 6 shows the eigenvalue variation in the rotor lead-lag modes and the torsion mode of the supporting structure as a result of an increase in the torsional stiffness (K_{ST}) of the supporting structure. The torsional stiffness K_{ST} was increased in increments from $K_{ST} = 1.59 \times 10^6$ N·m to 3.99×10^7 N·m., and the corresponding uncoupled nondimensional torsional frequencies ($\bar{\omega}_{ST}$) of the supporting structure are $\bar{\omega}_{ST} = 0.4$, 0.55, 0.846, 1.096, 1.2, 1.3, 1.4, 1.5, 1.754, 2.0. It is evident from the figure that the low-frequency lag mode 2 and high-frequency lag mode 2 remain unaffected during the variations in K_{ST}, and these modes are stable. In Fig. 6 the different curves are divided into three segments represented by points A, B, C, and D.

It is evident from Fig. 6 that in the range A to B, as the torsional stiffness K_{ST} is increased, the torsion mode of the supporting structure becomes increasingly stable and its frequency is increasing; the low-frequency lag mode 1 becomes increasingly unstable while its frequency increases slightly. This clearly indicates that the torsion mode is strongly coupled with the low-frequency lag mode 1. The high-frequency lag mode 1 experiences a slight increase in frequency, but its damping remains almost the same. In this range, A to B, the eigenvalues of these three modes have been distinctly identified based on their uncoupled nondimensional frequencies. In the range B to C, as the torsional stiffness K_{ST} is increased, the damping in the low-frequency lag mode 1 decreases and its frequency tends to increase toward 1.0. At the same time, the damping in torsional mode of the supporting structure decreases drastically, and a slight change in the frequency is observed (i.e., the frequency initially increases and then decreases). The high-frequency lag mode 1 shows an increase in frequency with no appreciable change in damping. In this range B to C, the eigenvalues of these three modes do not exhibit a direct one-to-one correspondence to the uncoupled nondimensional frequencies, implying that all these modes are coupled. Hence, in this range, B to C, the reference to the various modes as torsion mode, low-frequency lag mode 1, and high-frequency lag mode 1 is only for the convenience of explaining the variation of the eigenvalues. When the torsional stiffness K_{ST} is increased still further, i.e., in the range C to D, the eigenvalues start exhibiting a correspondence to nondimensional uncoupled frequencies indicating that these modes become slowly decoupled. In this range, C to D, the torsional mode of the supporting structure has low damping, and it tends to decrease asymptotically while the frequency increases from 1.5 to 1.75. The high-frequency lag mode 1 shows an increase in the frequency, and the mode becomes stable at the point D. The damping in the low-frequency lag mode 1 decreases, while the frequency undergoes a slight reduction. Beyond the point D, i.e., for $K_{ST} \geq 3.1 \times 10^7$ N·m, the eigenvalues of low-frequency lag mode 1 and high-frequency lag mode 1 show

negligible change, and the damping in torsion mode remains the same but its frequency increases. Beyond point D all three modes are stable.

An interesting observation that can be made from Fig. 6 is associated with the effect due to the increase in torsional stiffness K_{ST}. When K_{ST} is increased from 1.685×10^7 N·m to 3.99×10^7 N·m (in the range C to D and beyond), the eigenvalues corresponding to the high-frequency lag mode 1 tend to approach the eigenvalue corresponding to the high-frequency lag mode 2 (which remains unaffected during the variation in K_{ST}) and similarly the low-frequency lag mode 1 approaches the low-frequency lag mode 2. This behavior seems to indicate that as the torsional stiffness of the supporting structure is increased, the coupling between the two rotors due to the torsional deformation of the supporting structure is eliminated. As a result of this lack of coupling, the eigenvalues corresponding to the high-frequency lag modes 1 and 2 and low-frequency lag modes 1 and 2 approach each other.

The last observation that can be made from Fig. 6 is that the high-frequency lag mode 1, low-frequency lag mode 1, and torsion mode of the supporting structure undergo a reversal in their characteristics as K_{ST} is increased from 1.59×10^6 N·m to 3.99×10^7 N·m. Thus, the mode that was initially a distinct torsion mode becomes a low-frequency lag mode 1; the low-frequency lag mode 1 becomes a high-frequency lag mode 1, and the high-frequency lag mode becomes a torsion mode. For low and high values of the torsional stiffness—i.e., $K_{ST}\le1.59\times10^6$ N·m ($\bar{\omega}_{ST}<0.4$) and $K_{ST}\ge3.10\times10^7$ N·m ($\bar{\omega}_{ST}\ge1.754$), the torsional mode of the supporting structure, the low-frequency lag mode 1, and high-frequency lag mode 1 are all stable. For intermediate values of the torsional stiffness of the supporting structure, one of the lag modes is unstable.

The variation of the eigenvalues of the collective flap modes and body pitch mode due to increase in body inertia in pitch is presented in Fig. 7. It is evident from the figure that the pitch mode is a pure damped mode. An increase in pitch inertia causes the eigenvalues corresponding to the pitch mode to approach each other. The eigenvalues of the collective flap mode 1 tend to approach the eigenvalue of the collective flap mode 2. The pure damped nature of the pitch mode is associated with the presence of two rotors. During pitch motion, the net inflow in the two rotor systems changes. If in one rotor system the net inflow increases, then in the other the inflow decreases, and vice versa. These

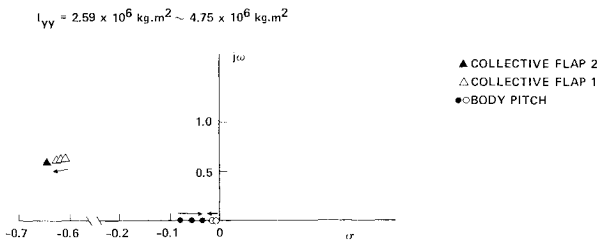

Fig. 7 Variation of nondimensional eigenvalues of blade collective flap modes and body pitch mode with increase in I_{yy} ($\bar{\omega}_{SBXY}=\bar{\omega}_{SBXZ}=2.192$, $\bar{\omega}_{ST}=1.754$, $I_{xx}=2.0\times10^6$ kg·m^2, $BR=0.792$, $C_T=0.00158$).

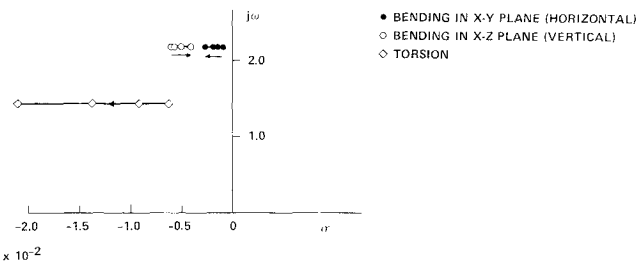

Fig. 8 Variation of nondimensional eigenvalues of the supporting structure elastic modes with decrease in buoyancy ratio, $BR=0.792$, 0.7, 0.6, 0.5 ($\bar{\omega}_{SBXY}=\bar{\omega}_{SBXZ}=2.192$, $\bar{\omega}_{ST}=1.754$, $I_{yy}=4.75\times10^6$ kg·m^2, $I_{xx}=2.0\times10^6$ kg·m^2).

Table 1 Coupling between various body modes and blade modes

	Lead-Lag modes						Flap modes					
	High freq.		Collective freq.		Low freq.		High freq.		Collective freq.		Low freq.	
Modes	1	2	1	2	1	2	1	2	1	2	1	2
Supporting structure symmetric bending in *x-y* (horizontal) plane		XXX				XX						
Supporting structure symmetric bending in *x-z* (vertical) plane	XXX		X		XX					X		
Supporting structure torsion (antisymmetric)	XXX				XXX							
Body pitch		X		X		X			X			
Body roll		X				XX						

Note: XXX = strongly coupled, XX = moderately coupled, X = weakly coupled.

Table 2 Equilibrium values at different buoyancy ratios

Buoyancy ratio, BR	θ_0, deg	β_0, deg	ζ_0, deg	ϕ_0, deg	λ	C_T
0.792	4.206	2.302	−3.963	−0.115	0.03272	0.00158
0.7	5.243	2.209	−5.074	−0.161	0.03820	0.00228
0.6	6.259	4.179	−6.453	−0.236	0.04313	0.00304
0.5	7.207	5.142	−7.994	−0.352	0.04743	0.00380

Note: $\bar{\omega}_{ST}=1.754$, $\bar{\omega}_{SBXY}=\bar{\omega}_{SBXZ}=2.192$, $I_{yy}=4.74\times10^6$ kg·m^2, $I_{xx}=2.0\times10^6$ kg·m^2

changes in inflow result in changes in the thrust in the two rotor systems. The rotor system that moves up during pitch motion experiences a reduction in thrust due to the increased inflow, and the rotor system that moves down produces more thrust due to the decreased flow. These changes in the thrust tend to restore the vehicle to its equilibrium position. Since this restoring force is proportional to the pitch rate, this mechanism produces a damping in pitch. In the present case, the pitch motion is overdamped. Hence, an increase in inertia causes the eigenvalues corresponding to the pitch mode to approach each other, as shown in Fig. 7.

The roll mode for the model vehicle is found to be a damped oscillatory mode. This is different from the pure damped mode[7] normally observed in a conventional tandem rotor helicopter. The reason for this oscillatory nature of the roll mode is due to the presence of the buoyancy of the envelope.

For all the cases analyzed, it was found that the flap and torsional modes of the rotor are always stable. The eigenvalues corresponding to the cyclic flap modes and all the torsion modes are not affected by the variation in the quantities used in this parametric study. The alternating modes of the rotor were also found stable.

The degree of coupling, as well as the relative strength of the coupling between the various blade modes and the body modes, is presented in a qualitative manner in Table 1. It is evident from this table that the supporting structure elastic modes are strongly coupled with the low-frequency and high-frequency lead-lag modes.

The effects of varying the buoyancy ratio on the stability of the vehicle are represented in Table 2 and Fig. 8. Table 2 shows the results from the trim analysis at various buoyancy ratios. As the buoyancy ratio is decreased, the equilibrium angles of the blade and the thrust coefficient of the rotors are increased.

Figure 8 depicts the variation of eigenvalues in supporting structure elastic modes with decrease in buoyancy ratio. The direction of arrows in the figure indicates the variation of the eigenvalues as a result of the decrease in buoyancy ratios. The frequencies corresponding to these modes are not affected by the variation in buoyancy ratio. However, the damping in bending in x-y plane increases, the damping in bending in x-z plane decreases, and the damping in torsion mode increases.

As the buoyancy ratio is decreased, one of the eigenvalues corresponding to the pitch mode decreases while the other eigenvalue increases. The pitch mode always remains a pure damped mode. The roll mode, which was initially a stable mode, becomes unstable for buoyancy ratios $BR \leq 0.6$.

The results obtained also indicate that as the buoyancy ratio is decreased, the damping in lead-lag modes of the rotor increases while the damping in flap and torsions modes of the rotor decreases. However, changes in the buoyancy ratio have only a minor effect on the frequencies of the blade modes. A quantitative indication of the magnitude of the changes in damping in the blade modes produced by changes in the buoyancy ratio is illustrated by the following results: for a 40% reduction in buoyancy ratio, the damping in torsion modes decreases by 12%; the damping in flap modes decreases by 12%, and the damping in lag modes increases by 200%.

V. Concluding Remarks

This paper presents the results of an aeromechanical stability analysis of a model vehicle representative of a HHLA configuration in hovering flight. The most important conclusions obtained in this study are presented below:

1) The rotor cyclic lead-lag modes couple strongly with the bending modes and the torsion mode of the supporting structure; as a consequence, the stability of the lead-lag modes is sensitive to changes in stiffness (or the natural frequencies) of the supporting structure in bending and torsion. Therefore the natural frequencies of the supporting structure must be designed so as to be well separated from the frequencies of the rotor lead-lag modes. This also emphasizes the importance of modeling the supporting structure with an adequate number of elastic modes.

2) The low-frequency and high-frequency lead-lag modes of the rotor and the torsion mode of the supporting structure undergo a change in their basic characteristics as the torsional stiffness of the supporting structure is increased from a low to a high value (i.e., $K_{ST} = 1.59 \times 10^6$ N·m to 3.99×10^7 N·m).

3) The lead-lag modes of the rotor are stable only when the torsional stiffness of the supporting structure has low or high values ($K_{ST} \leq 1.59 \times 10^6$ N·m and $K_{ST} \geq 3.10 \times 10^7$ N·m). For intermediate values of K_{ST}, one of the lead-lag modes is unstable.

4) The stability analysis of the coupled rotor/vehicle dynamics clearly illustrates the fundamental features of the aeroelastic stability of the rotor, the coupled rotor/support system aeromechanical stability, and the vehicle dynamic stability in longitudinal and lateral planes.

Appendix A

Blade Data

The HHLA model (Fig. 2) has identical rotors.

Type of rotor: Articulated rotor

Number of blades	N	4
Blade chord	$c = 2b$	41.654 cm
Hinge offset	e	30.48 cm
Rotor radius	R	8.6868 m
Rotor rpm	Ω	217.79 rpm

Aerodynamic Data

Blade airfoil		NACA 0012
Lift curve slope	a	2π
Lock number	γ	10.9
Solidity ratio	σ	0.0622
Density of air	ρ_a	1.2256 kg/m^3
Blade profile drag coefficient	c_{d0}	0.01

Nonrotating Blade Frequencies (Articulated Blade)

Flap frequency	ω_F	0
Lead-lag frequency	ω_L	0
Torsional frequency parameter	$\omega_T = (K_\phi / mR^3)^{1/2}$	(assumed) 1.895 rad/s
Damping in flap	g_{SF}	0
Damping in lead lag	g_{SL}	0
Damping in torsion	g_{ST}	0

Vehicle Data

Weight of fuselage F_1	W_1	3.5919×10^4 N
Weight of fuselage F_2	W_{F2}	3.5919×10^4 N
Weight of underslung load	W_{UN}	0.0
Weight of envelope	W_{EN}	8.5539×10^4 N
Weight of supporting structure	W_S	9.4302×10^3 N
Weight of passenger compartment [(Treated as a lumped structural load attached at the point 0_s on the structure (Fig. 2)]	W_S'	6.6723×10^3 N
Buoyancy on the envelope	P_z^s	1.3748×10^5 N

Geometric Data

Distance between origin O_s and F_1	ℓ_{F1}	−21.946 m

Distance between origin O_s and F_2	ℓ_{F2}	21.946 m
Distance between origin O_s and underslug load (assumed)	h_1	−15.24 m
Distance between centerline and rotor hub	h_2	2.591 m
Distance between centerline and center of volume of envelope	h_3	14.64 m
Distance between centerline and c.g. of the envelope	h_4	8.544 m
Distance between origin O_s and c.g. of the structure	h_5	0.0

Structural Dynamic Properties of the Supporting Structure

The supporting structure is modeled as an elastic structure with three normal modes of vibration: two normal modes for bending in vertical and in horizontal plane and one mode for torsion. The two bending modes are symmetric modes and the torsion is an antisymmetric mode. It was assumed that the envelope and the underslung load are attached to the supporting structure at the origin O_s. The data given above show that the vehicle is symmetric about Y-Z plane. Furthermore, due to the presence of a heavy mass attached at the center (O_s) of the supporting structure, the mode shapes in bending and torsion for each half of the model are assumed to be the modes of a cantilever with a tip mass.

Modal Displacement at F_1, F_2, and O_s

The symmetric mode shape in bending for each half of the supporting structure can be written as (Ref. 11, p. 140)

$$\eta_1\left(\frac{X}{L}\right)=6\left(\frac{X}{L}\right)^2-4\left(\frac{X}{L}\right)^3+\left(\frac{X}{L}\right)^4 \quad \text{(bending in } X\text{-}Y \text{ plane)}$$

and

$$\eta_2\left(\frac{X}{L}\right)=6\left(\frac{X}{L}\right)^2-4\left(\frac{X}{L}\right)^3+\left(\frac{X}{L}\right)^4 \quad \text{(bending in } X\text{-}Z \text{ plane)}$$

where X is the coordinate of any section of the supporting structure from origin O_s and L is the length of the supporting structure, $L=21.946$ m. The mode shape for torsion, for each half of the supporting structure, is (Ref. 11, p. 99)

$$\eta_3\left(\frac{X}{L}\right)=\sin\frac{\pi}{2}\left(\frac{X}{L}\right)$$

Generalized Mass and Stiffness Data

Generalized mass and generalized stiffness for the ith mode of vibration of the supporting structure are defined as

$$M=\int_{F1}^{F2} m\eta_i^2 \mathrm{d}x \text{ and } K=\omega_i^2 M,$$

respectively, where ω_i is the ith modal frequency, η_i is the ith mode shape, and m is the mass per unit length (for bending modes), or m is the mass moment of inertia per unit length (for torsion modes).

Bending in x-y plane (horizontal) generalized mass	M_{SBXY}	6.801×10^4 kg
Bending in x-z plane (vertical) generalized mass	M_{SBXZ}	6.801×10^4 kg
Torsion generalized mass	M_{ST}	1.936×10^4 kg·m^2

Acknowledgments

This work was supported by NASA Ames Research Center under Grant NAG 2-116. The authors would like to express their gratitude to the grant monitor Dr. H. Miura, NASA Ames Research Center, for providing a large part of the data used in these calculations, and also for his constructive comments and suggestions.

References

[1]Goodyear Aerospace Corp. "A Preliminary Design Study of a Hybrid Airship for Flight Research," NASA CR-166246, July 1981.

[2]Tischler, M. B., Ringland, R. F., and Jex, H. R., "Heavy-Lift Airship Dynamics," *Journal of Aircraft,* Vol. 20, May 1983, pp. 425-433.

[3]Venkatesan, C. and Friedmann, P. P., "Aeroelastic Effects in Multirotor Vehicles with Application to Hybrid Heavy Lift System, Part I: Formulation of Equations of Motion," NASA CR-3822, Aug. 1984.

[4]Friedmann, P. P., "Formulation and Solution of Rotary-Wing Aeroelastic Stability and Response Problems," *Vertica,* Vol. 7, No. 2, 1983, pp. 101-141.

[5]Greenberg, J. M., "Airfoil in Sinusoidal Motion in a Pulsating Flow," NACA TN-1326, 1947.

[6]Venkatesan, C. and Friedmann, P. P., "Aeroelastic Effects in Multirotor Vehicles, Part II: Method of Solution and Results Illustrating Coupled Rotor/Body Aeromechanical Stability," NASA CR report being reviewed for publication.

[7]Johnson, W., *Helicopter Theory,* Princeton University Press, Princeton, NJ, 1980.

[8]Levin, J., "Formulation of Helicopter Air-Resonance Problem in Hover with Active Controls," M.Sc. Thesis, Mechanics and Structures Department, University of California, Los Angeles, Sept. 1981.

[9]Friedmann, P. P. and Venkatesan, C., "Coupled Helicopter Rotor/Body Aeromechanical Stability Comparison of Theoretical and Experimental Results," *Journal of Aircraft,* Vol. 22, Feb. 1985, pp. 148-155.

[10]Venkatesan, C. and Friedmann, P. P., "Aeromechanical Stability Analysis of Multirotor Vehicle Model Representing a Hybrid Heavy Lift Airship," *Proceedings of the AIAA/ASME/ASCE/AHS 25th Structures, Structural Dynamics and Materials Conference,* May 14-16, 1984, Palm Springs, CA, pp. 251-265.

[11]Bisplinghoff, R. L., Ashley, H., and Halfman, R. L., *Aeroelasticity,* Addison-Wesley, Reading, MA, 1955.

[12]Aviation Week and Space Technology, Feb. 20, 1984, p. 53.